Observation of ion cyclotron range of frequencies mode conversion plasma flow drive on Alcator C-Mod

Observation of ion cyclotron range of frequencies mode conversion plasma flow drive on Alcator C-Mod[a)]

Y. Lin,[b)] J. E. Rice, S. J. Wukitch, M. J. Greenwald, A. E. Hubbard, A. Ince-Cushman, L. Lin, E. S. Marmar, M. Porkolab, M. L. Reinke, N. Tsujii, J. C. Wright, and Alcator C-Mod Team
Plasma Science and Fusion Center, Massachusetts Institute of Technology, Cambridge, Massachusetts 02139, USA

(Received 4 December 2008; accepted 26 January 2009; published online 11 March 2009)

At modest ^{3}He levels ($n_{3\mathrm{He}}/n_e \sim 8\%-12\%$), in relatively low density D(^{3}He) plasmas, $\bar{n}_e \leq 1.3\times 10^{20}$ m^{-3}, heated with 50 MHz rf power at $B_{t0} \sim 5.1$ T, strong (up to 90 km/s) toroidal rotation (V_ϕ) in the cocurrent direction has been observed by high-resolution x-ray spectroscopy on Alcator C-Mod. The change in central V_ϕ scales with the applied rf power (≤ 30 km s^{-1} MW^{-1}), and is generally at least a factor of 2 higher than the empirically determined intrinsic plasma rotation scaling. The rotation in the inner plasma ($r/a \leq 0.3$) responds to the rf power more quickly than that of the outer region ($r/a \geq 0.7$), and the rotation profile is broadly peaked for $r/a \leq 0.5$. Localized poloidal rotation ($0.3 \leq r/a \leq 0.6$) in the ion diamagnetic drift direction (~ 2 km/s at 3 MW) is also observed, and similarly increases with rf power. Changing the toroidal phase of the antenna does not affect the rotation direction, and it only weakly affects the rotation magnitude. The mode converted ion cyclotron wave (MC ICW) has been detected by a phase contrast imaging system and the MC process is confirmed by two-dimensional full wave TORIC simulations. The simulations also show that the MC ICW is strongly damped on ^{3}He ions in the vicinity of the MC layer, approximately on the same flux surfaces where the rf driven flow is observed. The flow shear in our experiment is marginally sufficient for plasma confinement enhancement based on the comparison of the $E\times B$ shearing rate and gyrokinetic linear stability analysis. © *2009 American Institute of Physics*.
[DOI: 10.1063/1.3082936]

I. INTRODUCTION

Plasma rotation (flow) and velocity shear can be important in stabilizing micro- and macroinstabilities [such as drift wave turbulence[1,2] or resistive wall modes[3] (RWMs)] in tokamak plasmas. There are, in general, two types of rotation according to their source: intrinsic and externally driven. Intrinsic rotation exists independent of the external momentum drive or auxiliary heating methods, and is observed on many tokamaks (see Ref. 4 for a recent intermachine study on intrinsic rotation). On Alcator C-Mod, intrinsic rotation has been observed in plasmas with Ohmic heating,[5] ion cyclotron range of frequencies (ICRF) minority heating[6] (MH) in both upper and lower single null and double null magnetic configurations.[7] The rotation velocity is found to strongly correlate with plasma parameters, for example, $\Delta V_\phi \propto \Delta W/I_p$,[8] where ΔV_ϕ is the change in toroidal velocity, ΔW is the change in plasma stored energy, and I_p is the plasma current. Extrapolating from a database of observations in existing tokamaks, the intrinsic rotation on ITER might be up to the level of several hundreds of km/s.[4] Such a rotation magnitude is possibly sufficient for RWM stabilization, but an intrinsic rotation actuator for active plasma control is expected to be limited due to its correlation to plasma pressure and lack of profile control. For externally driven rotation, neutral beam injection is the main method on present-day major tokamaks. The central toroidal rotation is about 20–30 km s^{-1} MW^{-1} beam power in large tokamaks such as Japan Atomic Energy Research Institute Tokamak-60 Upgrade[9] (JT60-U) and Joint European Torus[10] (JET), and 50–60 km s^{-1} MW^{-1} in medium-sized tokamaks such as ASDEX-Upgrade[11] and DIII-D.[12] However, for ITER and future reactors, the beam energy will be significantly higher in order to penetrate the expected higher density plasma and larger machine size. This will result in a lower torque per megawatts beam power. Combined with a much larger inertia, beam driven rotation is expected to be small on ITER. For instance, assuming $\chi_\phi \approx \chi_i$, simulations find that the beam driven toroidal rotation may be in the range of 1–2 km s^{-1} MW^{-1} for the 1 MeV NB on ITER.[13] Since χ_ϕ and the possibility of a momentum pinch will be the determining factors for the achievable rotation velocity at given torque, estimating χ_ϕ on ITER is an active research area. However, regardless the value of χ_ϕ, beam driven rotation profile is dictated by beam penetration and deposition profile, which offer little direct profile controllability.

Externally launched electromagnetic radio frequency (rf) waves may offer another means of controlling flow on ITER and reactors. If the rf flow drive can be localized, this may also offer a unique means for manipulating transport via flow shear stabilization—thus affecting pressure profiles, bootstrap current, etc. Many efforts have been made in searching for an efficient rf flow drive method that may also be applicable on ITER and beyond. Experimentally, ICRF minority

[a)]Paper BI2 6, Bull. Am. Phys. Soc. **53**, 23 (2008).
[b)]Invited speaker. Electronic mail: ylin@psfc.mit.edu.

heated and electron cyclotron heated plasmas show no evidence of direct rf driven rotation, for example, ICRF MH on Alcator C-Mod,[8] JET,[14] Tore-Supra,[15] etc., and EC heated plasmas on DIII-D,[16] JT-60U[17] and Tokamak à Configuration Variable (TCV).[18] Recently, lower hybrid current drive has been shown to cause a reduction in the usual intrinsic cocurrent rotation on Alcator C-Mod on the current diffusion time scale.[19] Kinetic Alfvén waves were observed to drive plasma flow on the Phaedrus-T tokamak.[20] Poloidal flow driven by direct launch ion Bernstein waves (IBWs) was detected on Tokamak Fusion Test Reactor (TFTR).[21,22] Fast magnetosonic waves (fast wave, or FW) were shown to directly drive toroidal rotation on JET,[23] but the observed toroidal rotation was small. Using ICRF mode conversion (MC), some preliminary evidence of poloidal flow drive (≤ 1 km/s at 2 MW rf power) was observed between the MC surface and ion cyclotron (IC) layer on TFTR,[24] but no further experiment was conducted. Here we report the first definite demonstration and detailed study of efficient toroidal rotation (V_ϕ) and poloidal rotation (V_θ) generation via the ICRF MC process in tokamaks.[25]

The paper is organized as follows. In Sec. II, the experimental setup, diagnostics and simulation tools are described. In Sec. III, we compare the rotation observation in ICRF MH and MC plasmas, and also the characteristics of the MC driven flow. In Sec. IV, we present wave detection and full wave rf simulations, and also show the correlation between the MC ion heating and flow drive, followed by discussion in Sec. V and summary in Sec. VI.

II. EXPERIMENTAL SETUP, DIAGNOSTICS, AND SIMULATION TOOLS

In previous studies, the rotation in the ICRF MH plasmas on Alcator C-Mod has been found to follow the same empirical scaling as that in Ohmic plasmas, suggesting that the rotation in ICRF MH plasmas is intrinsic. To demonstrate a flow drive mechanism that differs from the intrinsic rotation, we ran plasmas with the same density, magnetic field, and similar power deposition location with MC heating. To avoid complication from the large intrinsic rotation associated with high confinement mode (*H*-mode), we ran plasmas in the upper-single-null shape, which has a higher low confinement mode (*L*-mode) to *H*-mode transition power threshold (∇B drift in the unfavorable direction), and maintained the discharges in *L*-mode. In Fig. 1, the scenarios of two typical plasmas in this experiment are shown. The MH plasma consists of D majority and H minority ($n_H/n_e \sim 3\%-5\%$), with FWs of 80 MHz launched from the low field side (LFS) of the tokamak (major radius $R=0.67$ m and minor radius $a=0.22$ m). At $B_{t0}=5.1$ T, the H cyclotron resonance at 80 MHz is located at $R \approx 0.65$ m (magnetic axis at 0.68 m). For the MC heating, we launch FWs at 50 MHz into D majority and ^{3}He minority plasmas, where the ^{3}He cyclotron resonance layer is at $R \approx 0.70$ m at $B_{t0}=5.1$ T. As shown in the figure, we define δ as the separation between the IC resonance layer and the hybrid layer (defined as $n_\parallel^2=S$, where S is the usual Stix parameter,[26] and $n_\parallel$ is the parallel index of refraction of the FW), and define

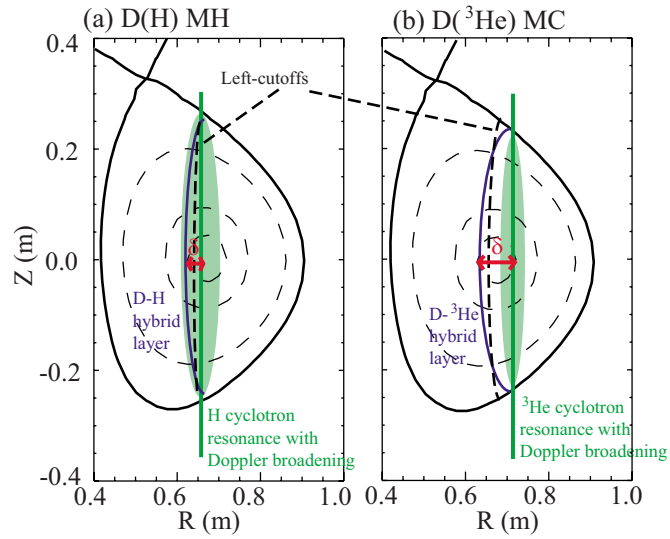

FIG. 1. (Color online) Plasma configuration for the experiment (a) D(H) MH at 80 MHz; (b) D–^{3}He MC heating at 50 MHz. Both plasmas have $B_{t0}=5.1$ T, and in upper-single-null.

$\Delta \propto k_\parallel v_{ti} R/\omega$ as the Doppler width of the cyclotron resonance layer. The ratio δ/Δ largely determines whether MH or MC dominates the heating process.[27] At small δ/Δ, as shown in the MH plasma of Fig. 1(a), the FW deposits most of its power to the minority ions through ion resonance heating, and the generated energetic ions then slow down and transfer power to the bulk ions and electrons. At larger δ/Δ, like the scenario in Fig. 1(b), at $n_{He3}/n_e \sim 10\%$ (^{3}He gas is puffed externally), the IC resonance for the FW does not overlap the hybrid layer (also called MC surface in this case), and the FW undergoes MC and becomes the MC ion cyclotron wave (ICW) and MC IBW near the MC surface. The MC IBW, existing near the midplane, propagates to the high field side (HFS) and heats electrons via Landau damping (it would interact with D ions if it reaches the vicinity of the D IC layer). The MC ICW, existing vertically some distance away from the midplane, propagates toward the LFS. The MC ICW can be mostly absorbed by electrons via Landau damping, or mostly by the ^{3}He ions if the wave is near the ^{3}He cyclotron resonance layer.[28,29]

In previous MC experiments on Alcator C-Mod, the FW and mode converted waves (IBW and ICW) have been detected by a phase contrast imaging (PCI) system set up in the heterodyne mode,[28,30] and this technique is also utilized in the flow drive experiments (Fig. 2). The laser of the PCI system is modulated at a frequency near the rf frequency so that the rf field induced coherent density oscillations appear in the detector signal at the beat frequency. This setup can provide the structure of the MC waves along vertical channels (i.e., versus major radius R) and also k_R, the wave number in the R direction. The direct electron heating deposition profile, a signature of the MC process, is calculated from the break-in-slope of the electron temperature traces from electron cyclotron emission (ECE) diagnostics.[31] The PCI measured wave structure and electron power deposition are compared to simulations using the two-dimensional (2D) full wave code TORIC (Refs. 32 and 33) to identify the power

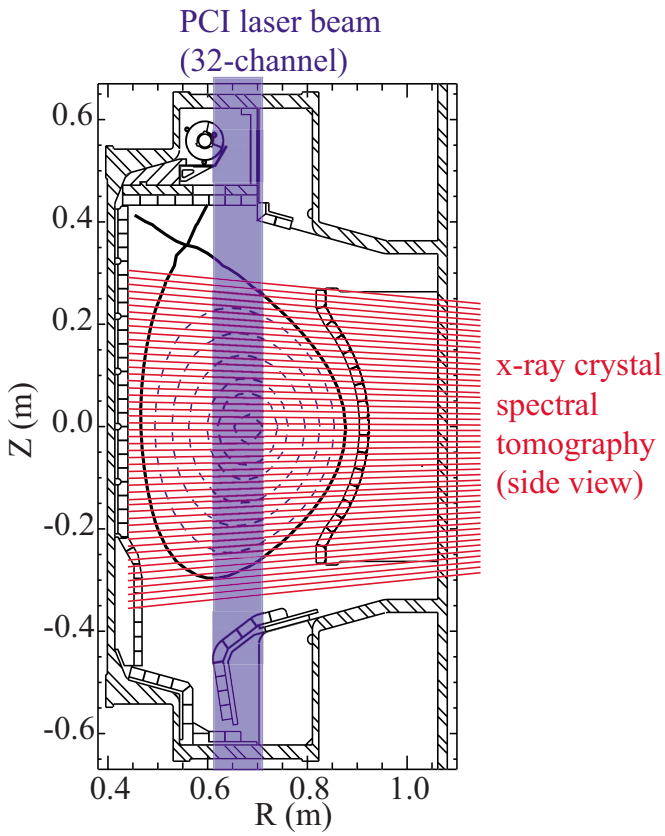

FIG. 2. (Color online) Layout of the PCI system (vertical laser beam) and x-ray crystal spectral tomography system (side view).

deposition profiles from the waves. TORIC solves the finite Larmor radius wave equations in 2D toroidal geometry using a spectral ansatz. Magnetic equilibria reconstructed by equilibrium fitting (EFIT) (Ref. 34) are also implemented in our simulations to better represent the experimental conditions.

Plasma rotation is measured from the Doppler shift of the H-like and He-like argon line emission in the wavelength range of 3.7–4.0 Å by a novel spatially resolving x-ray crystal tomography system.[35] Unlike charge exchange recombination spectroscopy, the system is passive and does not require a neutral beam. It utilizes a spherically bent quartz crystal and a set of 2D x-ray detectors to image the entire plasma cross section with a spatial resolution about 1 cm (Fig. 2), and frame rate up to 200 Hz. There are two viewing chords on a flux surface, above and below the midplane. The viewing arrays are aligned with an 8 degree angle toroidally so that the "common mode" of the two viewing chords is sensitive to the toroidal rotation, while the "differential mode" is sensitive to the poloidal rotation. Rotation profile can be obtained by tomographically inverting the line measurements assuming constant rotation frequency on a magnetic flux surface. Additionally, the instrument also provides impurity temperature measurement from the width of the spectroscopic lines.

To study the effect of the flow shear on turbulence suppression, we use the gyrokinetic code GYRO (Ref. 36) for linear stability analysis, and compare the result with the $E\times B$ shear generated by the plasma rotation.

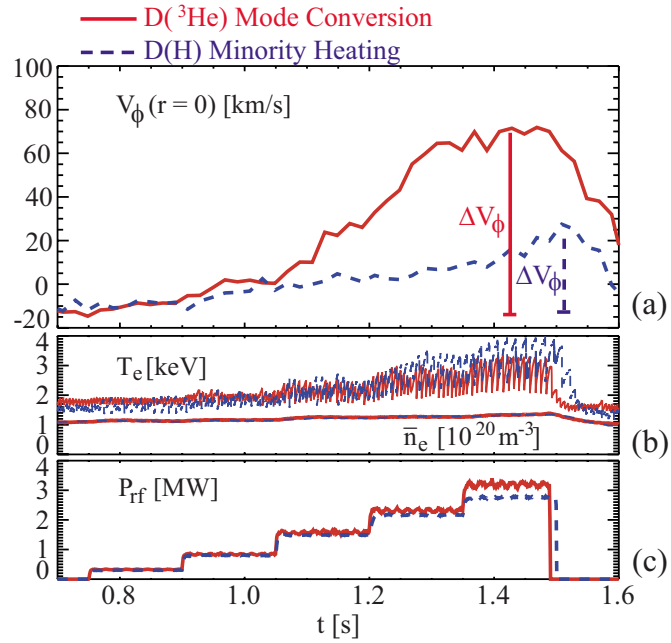

FIG. 3. (Color online) Data traces comparison of the MH plasma (blue dashed line) and MC plasma (red solid line): (a) Central toroidal rotation; (b) T_e and n_e; (c) $P_{\rm rf}$.

III. ROTATION IN ICRF MODE CONVERSION HEATED AND MINORITY HEATED PLASMAS

In Fig. 3, the central toroidal velocity V_ϕ $(r=0)$ from the two plasmas in Fig. 1 is shown. As shown in Fig. 3(a), ΔV_ϕ $(r=0)$ in the MC plasma is more than a factor of 2 larger than that in the MH plasma for the same power level [Fig. 3(c)]. In the MC plasma, central V_ϕ rises from -10 km/s (countercurrent direction), a typical value in Ohmic L-mode plasmas, to +75 km/s (110 krad/s, and $M_A=V_\phi/C_A\sim 0.013$, where M_A is the Alfvén Mach number and C_A is the Alfvén velocity) in the cocurrent direction with 3 MW rf power. In contrast, in the MH plasma with nearly identical rf power trace, V_ϕ $(r=0)$ only rises to +20 km/s. For intrinsic rotation, previous studies showed that the rotation first starts to rise from the edge, and the core rotation follows.[37] In MC

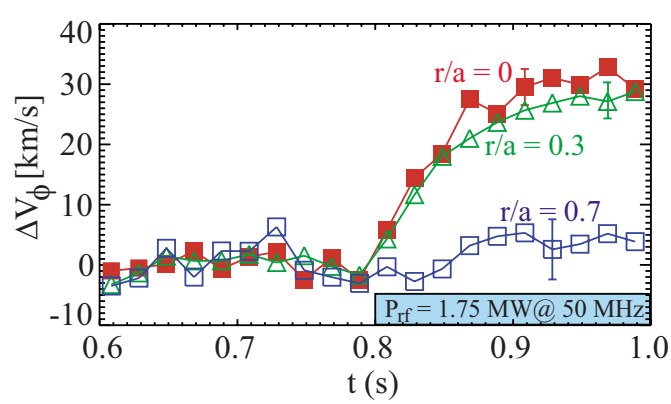

FIG. 4. (Color online) Change in toroidal rotation velocity at different viewing chords responding to the application of rf power at 0.8 s.

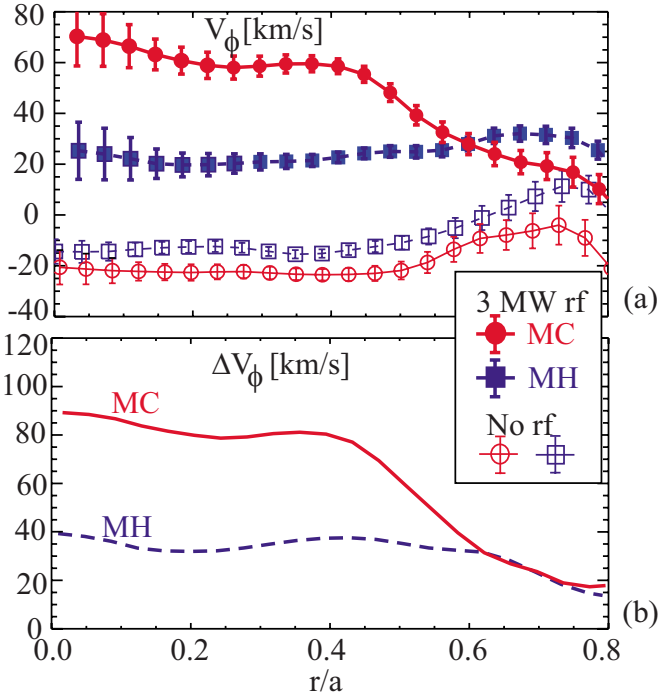

FIG. 5. (Color online) (a) Tomographically inverted toroidal rotation profiles (on the midplane on the LFS of the axis) for the MC and MH plasmas shown in Fig. 3; (b) The difference of rotation with and without rf power.

flow drive experiments, the rotation first appears in the plasma core, as show in Fig. 4. The rotation at $r/a=0$, and 0.3 responds to the power immediately, and rises to a steady level in less than 80 ms (about the time scale of momentum confinement time τ_ϕ), while the rotation in the outer channel is delayed and also has a much smaller response. The resulting rotation profile for MC flow drive experiments is also significantly different from the profile resulting from intrinsic rotation. In Fig. 5 we compare the tomographically inverted toroidal rotation profiles for the MH and MC plasmas in Fig. 3. The plotted rotation velocity is the value on the midplane on the LFS of the magnetic axis, while we assume the rotation frequency to be constant on a flux surface. At $t=1.4$ s with about 3 MW rf power, the rotation profile in the MC plasma is broadly peaked for $r/a<0.45$, while the profile in the MH plasma is flat (typical in L-mode plasmas with intrinsic rotation). Figure 5(b) suggests a factor of more than 2 difference in the change in rotation in the region of $r/a<0.4$. The changes in total plasma angular momentum are 9×10^{-2} and 5×10^{-2} kg m^2 s^{-1} respectively, assuming the same change in main ion rotation as the impurity rotation.

The change of rotation velocity in the MH plasmas follows the well-established empirical $\Delta W/I_p$ scaling,[8] as shown in Fig. 6(a), and the rotation in MC plasma is generally at least a factor of 2 above the intrinsic rotation scaling. When plotted versus P_{rf}/n_e as in Fig. 6(b), the velocity change ΔV_ϕ in the MC plasmas is approximately linear with the applied rf power level, an indication that the rf effect is through the rf power, but not through the field strength.

Concomitant to the strong toroidal rotation, a poloidal rotation V_θ in the ion diamagnetic direction is observed in the

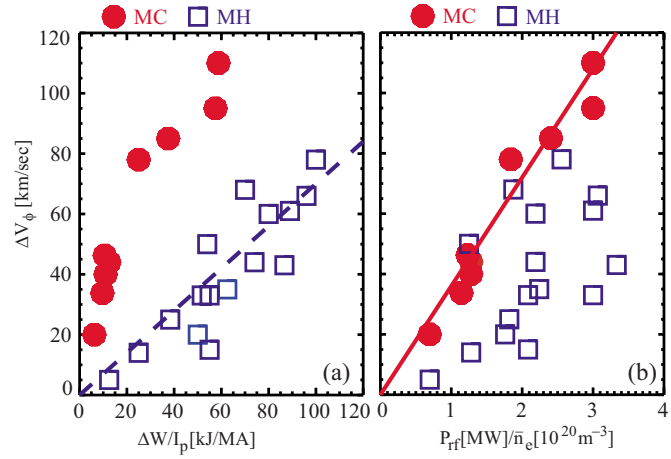

FIG. 6. (Color online) Toroidal rotation scaling: (a) ΔV_ϕ vs intrinsic rotation scaling law $\Delta W/I_p$; (b) ΔV_ϕ vs P_{rf}/n_e. Lines are linear fits of the data.

MC plasma. In Fig. 7, ΔV_θ (velocities prior to the rf application is subtracted) at different rf power levels in the MC and MH plasmas is compared. In the MH plasma, there is no detectable change in poloidal rotation (less than the diagnostic uncertainties) in the entire region covered, while in the MC plasma, significant rotation appears in the region of $0.3<r/a<0.6$, and peaks at ~2 km/s in the ion diamagnetic drift direction at 3 MW rf power. The rotation velocities measured by the spectrometer are from argon impurity rotation, and the main ion rotation can be different. The existence of the main ion rotation can be inferred from the density fluctuation spectra measured by the PCI. The density fluctuation spectra are significantly broadened following the trend of poloidal rotation shown in Fig. 8. Either toroidal rotation or poloidal rotation, or a combination can introduce such Doppler broadening, thus we cannot separate their effects experimentally. In order to better measure mode con-

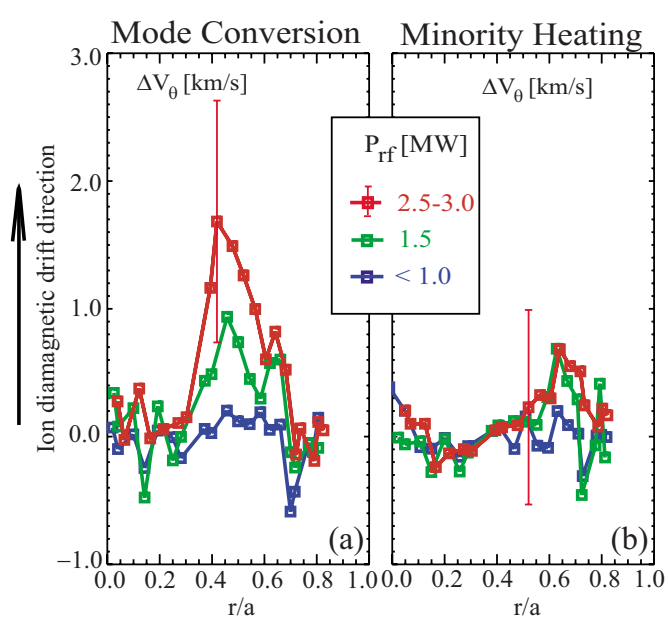

FIG. 7. (Color online) Change in poloidal rotation profile (Ohmic V_θ is subtracted) at different rf power levels: (a) MC; (b) MH.

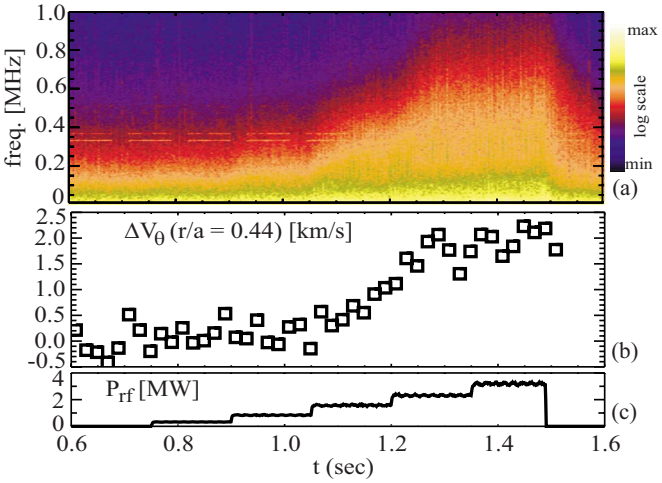

FIG. 8. (Color online) (a) Spectra vs time of density fluctuations measured by PCI; (b) poloidal rotation trace at $r/a=0.44$; (c) P_{rf}.

verted rf waves (see Sec. IV), the PCI system was not set up to have vertical localization capability.[38] As a result, the direction of the main ion rotation cannot be determined from the PCI fluctuation data.

However, if we assume all the broadening is from the polodial rotation, and use $k_\theta \approx k_R \sim 5\ \text{cm}^{-1}$, as measured by PCI, the broadening in the turbulence spectra would indicate ~ 4 km/s main ion poloidal rotation.

We have also studied the parameter dependence of the flow drive efficiency, including antenna toroidal phase, ^{3}He level, and B field. In Fig. 9, we show the rotation traces in a plasma where the antenna phase of the 50 MHz rf power is varied in time: +90° (wave cocurrent), 180° (dipole), and

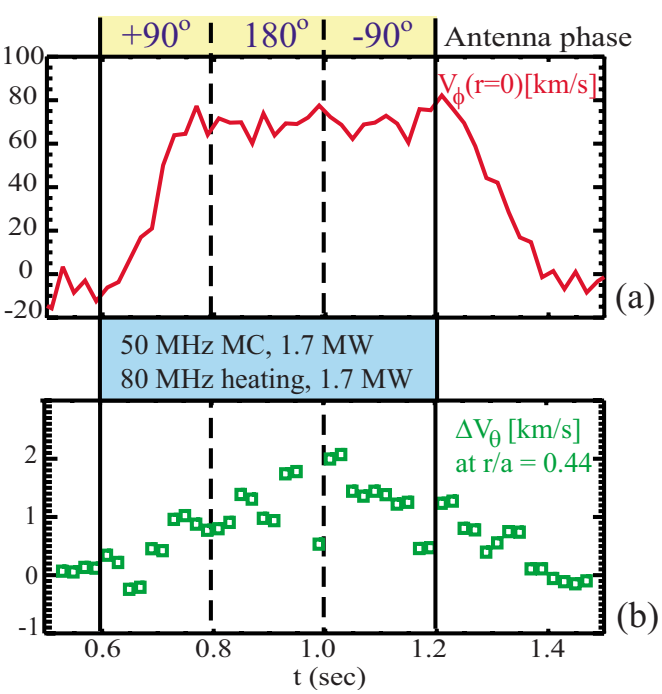

FIG. 9. (Color online) Antenna phase dependence of rotation: (a) V_ϕ; (b) ΔV_θ. The antenna phase of the 50 MHz rf is labeled at the top. Total rf power 3.4 MW (1.7 MW at 50 MHz and 1.7 MW from 80 MHz) at $t=0.6-1.2$ s.

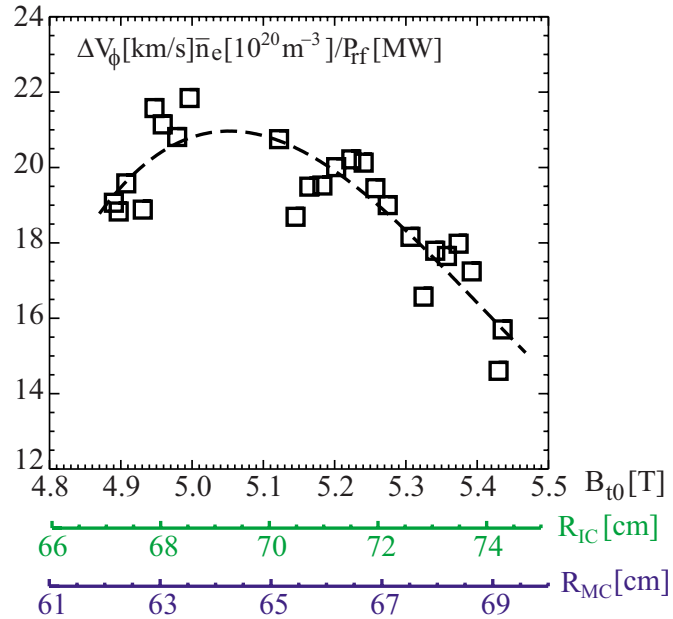

FIG. 10. (Color online) Flow drive efficiency vs B field. The corresponding major radii of IC resonance (R_{IC}) and MC (R_{MC}) are also indicated. Magnetic axis at $R=68$ cm. The dashed line is an order of three polynomial fit of the data points.

−90° (wave countercurrent). While the rotation, both toroidal and poloidal, needs a time scale similar to the momentum diffusion time to reach the steady-state level, the changes in the antenna phase do not induce significant changes in rotation. More specifically, the rotation directions are the same at different antenna phase (V_ϕ in cocurrent and V_θ in ion diamagnetic drift direction), and their magnitudes are largely phase independent. As seen from a series of plasmas, +90° toroidal phase produces slightly larger toroidal rotation, but the differences in flow drive efficiency among different phases are fairly small (<10%). In terms of the effect of the ^{3}He level, we find the toroidal rotation at the high ^{3}He concentration level (~20%) or low ^{3}He level (~5%) is experimentally indistinguishable from the intrinsic rotation while a more detailed species concentration scan has yet been performed. The rotation is also found to depend on the B field when the ^{3}He level is kept constant. In Fig. 10, we show the result from a plasma discharge with B field ramping up and ramping down. The highest flow drive efficiency is found at $B_{t0} \sim 5-5.1$ T, where the ^{3}He IC resonance is close to the magnetic axis, and the MC surface several centimeters on the HFS of the axis.

IV. DETECTION OF MODE CONVERTED WAVES AND COMPARISON TO TORIC SIMULATIONS

In the MC plasmas for flow drive experiments, the PCI system was configured in the heterodyne mode and the MC waves have been detected. As shown in Fig. 11, the MC waves are ~1.5–3.5 cm on the HFS of the magnetic axis, and ~3–5 cm on the HFS of the ^{3}He resonance layer. The wave number k_R is in the range of 3–7 cm^{-1}, which is consistent with previous observations of the MC ICW in D–^{3}He plasmas in Alcator C-Mod and also the solution of the

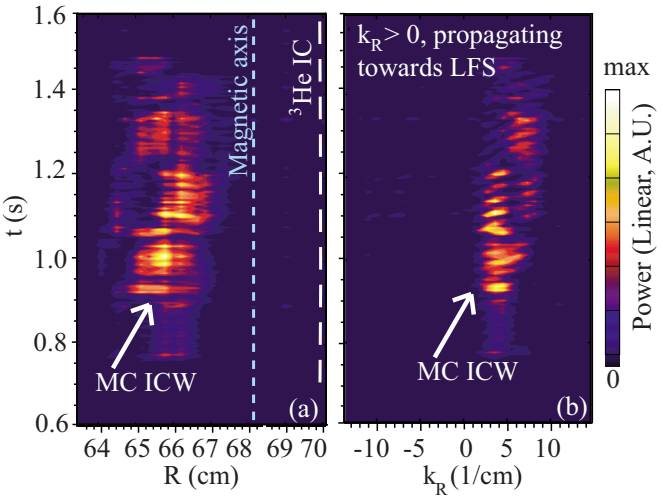

FIG. 11. (Color online) Mode converted waves measured by PCI of the MC plasma shown in Fig. 3: (a) amplitude (in terms of density fluctuation) vs time and major radius; (b) k-spectra vs time.

plasma dispersion equation.[30] In Fig. 12 we show the direct electron heating profile from the break in slope of temperature traces[31] at the fast power shut-off at $t \approx 1.48$ s of the MC plasma in Fig. 3. The result is a rather localized deposition profile peaked around $r/a=0.2$, and the total integrated power is about 0.4 MW out of total 3 MW launched from the antenna.

TORIC code calculates the wave fields and also the power deposition profiles via different absorption mechanisms. We do not have accurate measurement of $n_{3\mathrm{He}}/n_e$; instead, the value of the concentration is inferred from matching the TORIC simulated wave structure with PCI measurement, and also the TORIC electron deposition profile with electron deposition profile from ECE (Fig. 12). The resulted estimate of $n_{3\mathrm{He}}/n_e$ is in the range of 8%–12%. The most interesting feature from the simulation of this plasma is that the MC ICW deposits a significant portion of power to the ^{3}He ions through cyclotron resonance while most direct electron heating is from electron Landau damping of the MC IBW near the midplane. The 2D power deposition of the wave power to ^{3}He ions is shown in Fig. 13(a). The FW is only weakly absorbed at the ^{3}He resonance, while significantly more power is absorbed by the ^{3}He ions via the MC ICW. The interaction of the MC ICW with ^{3}He can be understood as a result of $k_\parallel$ upshift by the MC process, i.e., the $k_\parallel$ of the MC ICW is $\sim$40–50 m^{-1}, as calculated from the full electromagnetic dispersion equation, while the $k_\parallel$ of the FW is $\sim$10 m^{-1}. The upshifted $k_\parallel$ effectively broadens the ^{3}He cyclotron resonance layer, and causes the ion absorption of the MC ICW in the vicinity of the MC surface. Since the MC surface is approximately a vertical surface that intersects with a number of flux surfaces and the ICW exists vertically away from the midplane, the flux surface averaged power deposition to ^{3}He is broadly peaked in the region of $0.2 < r/a < 0.6$ [Fig. 13(b)], in the same region where significant flow is observed (cf. Figs. 5 and 7). This similarity suggests that the rf power to the ions from the MC ICW (a slow wave) may be the main flow drive mechanism, while on the other hand, the substantially more localized direct electron heating by the MC waves (Fig. 12) implies a lesser role of direct electron heating in contributing to flow drive.

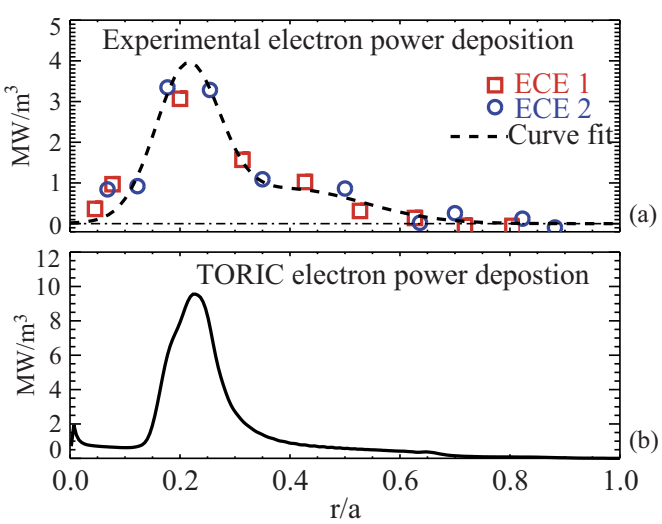

FIG. 12. (Color online) Direct rf power to electrons: (a) direct electron heating profile calculated from break-in-slope of ECE signals; (b) deposition profile from TORIC simulation ($n_{3\mathrm{He}}/n_e=0.08$).

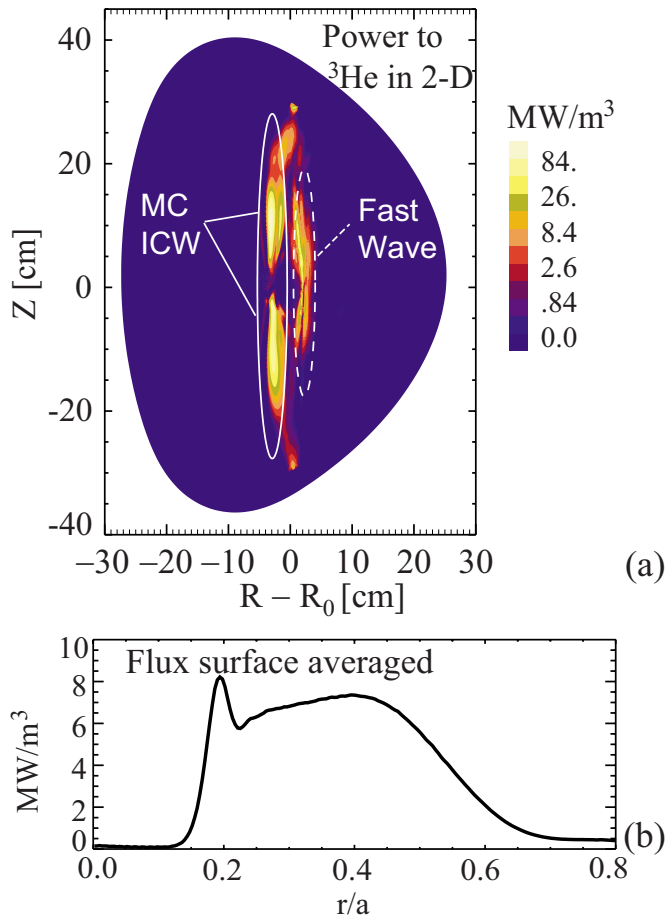

FIG. 13. (Color online) Direct power to ^{3}He ions: (a) 2D power deposition from TORIC simulation with FW and MC ICW labeled; (b) flux surface averaged profile.

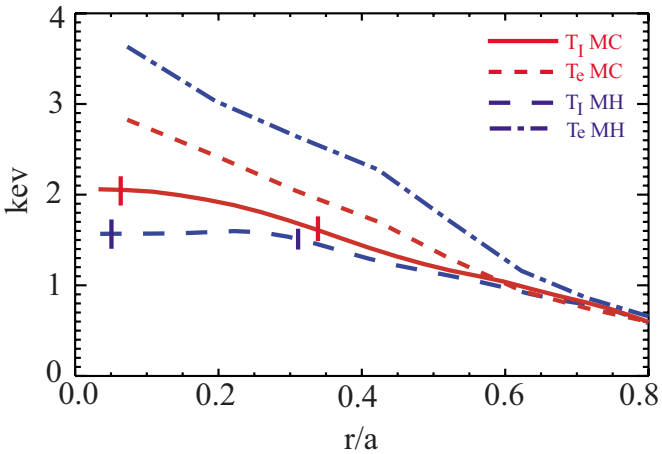

FIG. 14. (Color online) Argon impurity temperature from the x-ray spectra measurement and electron temperature from ECE ($t=1.4$ s of the plasmas shown in Fig. 3, averaged over two sawtooth periods).

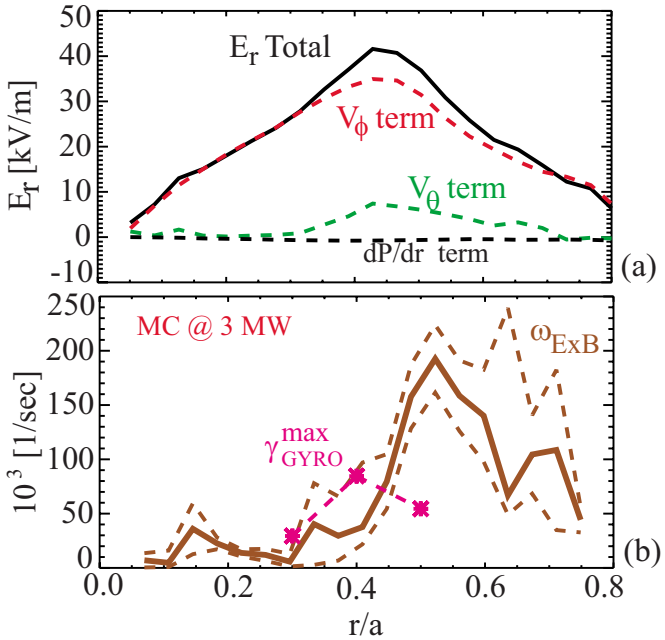

FIG. 15. (Color online) (a) Radial electric field E_r profile; (b) $E\times B$ shearing rate $\omega_{E\times B}$ (brown solid and dashed lines), and maximum linear growth rate from GYRO ($t=1.4$ s of the MC plasma shown in Fig. 3).

V. DISCUSSION

The involvement of slow wave and resonant wave-ion interaction for flow drive has been suggested by previous theoretical work on rf flow drive.[39–42] In previous attempts of MC flow drive experiments on Alcator C-Mod, e.g., as that reported in Ref. 43, we were not able to obtain conclusive evidence of flow drive, partially due to running plasmas with predominantly MC electron heating. Analytical estimates for V_ϕ and V_θ generated by direct launch IBW at the diffusive limit were presented in Ref. 39 and they are comparable to our experimental result.[25] However, the MC process is far more complicated than direct launch IBW, and the agreement could be fortuitous. The weak dependence of the rotation direction vs. antenna toroidal phase indicates the net wave toroidal momentum may not be crucial or it may be redistributed in the plasma in a preferential direction through complicated wave-plasma interaction. The up-down asymmetry of the MC ICW (Refs. 30 and 42) may provide a key to understanding such a preferential direction of the flow drive direction because the MC process to the ICW is strongly affected by the poloidal field direction (in other words, the direction of the plasma current). The immediate response of rotation at the plasma center suggests that the flow is a direct rf effect, and this may exclude theoretical models solely based on momentum generation from the plasma edge to interpret our observation. Previous modeling on MC flow drive[42] was on a different MC scenario ($B_{t0}=5.8$ T, and 80 MHz rf, and ion species mix 33%H, 23% ^{3}He, 21%D, and MC near the ^{3}He–H hybrid layer), and sheared flow drive force was calculated. The result was small and consistent to the particular plasma discharge modeled. Dedicated theory and modeling are required to further understand the flow drive mechanism, including the partition of power among different waves, the up-down asymmetry of the MC ICW, and the generation of flow driving force and momentum distribution.

On ITER and other future burning plasma devices, ICRF MC can be utilized in H–^{3}He plasmas during the nonradioactive phase and in *D-T* plasmas during the radioactive phase. However, because of the much larger machine size of ITER and higher electron temperature, the MC efficiency will generally be lower than that in Alcator C-Mod. The larger size increases the thickness of evanescent layer (relative to the wavelength) between the left-cutoff surface ($n_\parallel^2=L$, where L is a Stix' parameter[26]) and the MC surface, thus reducing the portion of FW power that tunnels through the evanescent layer for MC. This issue can be avoided by launching the FW from the HFS where no left-cutoff exists before the FW reaches the MC surface (cf. Fig. 1). This scenario has been confirmed to have higher MC efficiency than LFS launch by some preliminary TORIC simulation with ITER geometry. The higher T_e on ITER would substantially enhance power absorption by electrons through FW electron Landau damping,[44] thus leaves less power for MC. Moreover, higher T_e would also lead the MC process more toward the MC IBW, which deposits power onto electrons. In summary, extrapolating to ITER requires further experimental studies on Alcator C-Mod and other existing tokamaks equipped with ICRF capabilities.

In addition to the substantial difference observed in plasma rotation, the temperatures of the MH and MC plasmas are also different. In Fig. 14, we compare the argon impurity temperature and electron temperature from ECE of the two plasmas in Fig. 3 at $t=1.4$ s, and find that T_I in the MC plasma is higher for $r/a<0.5$, while for T_e the opposite holds. In this relatively low density L-mode plasma, the ion and electron equilibrium time $\tau_{ei}\geq 20$ ms at $r/a<0.5$, similar to the energy confinement time. As a result, the difference in rf power deposition schemes can partially explain the different behaviors in temperature. For the MH plasma, the energy of the H ion tails may have exceeded the critical energy and deposit more power to electrons than to bulk ions, while in the MC plasma, there is no energetic tail, and the tempera-

tures reflect the direct rf power deposition to ions and electrons. The deviation of the two ion temperatures at $r/a<0.5$ might also be an indication of the effect of the sheared flow on ion thermal transport. A detailed transport analysis will be required for this task. Here we present some preliminary linear analysis to show such a possibility. From the toroidal and poloidal rotation profiles, we can calculate the radial electrical field (E_r) profile from the radial force balance equation [Fig. 15(a)], and then calculate the $E\times B$ shearing rate, $\omega_{E\times B}$, using the Hahm–Burrell formula[45] [Fig. 15(b)]. For the MC plasma shown in Fig. 3, the maximum E_r is about 40 kV/m at $r/a\approx 0.45$, and $\omega_{E\times B}$ is peaked at 2×10^5 s^{-1} at $r/a\approx 0.5$, same location as the maximum toroidal rotation shear. By comparing $\omega_{E\times B}$ to the maximum growth rate $\gamma^{\max}$ obtained from GYRO (Ref. 36) linear stability analysis, we find that in the region of the large flow shear, $\omega_{E\times B}$ is similar or even larger than $\gamma^{\max}$. Although the effect of the $E\times B$ shear on turbulence suppression and transport needs to be further analyzed, the magnitude of $\omega_{E\times B}$ suggests that the available rf power on Alcator C-Mod is marginally sufficient for detailed transport study using the MC flow drive.

VI. SUMMARY

ICRF MC driven toroidal and poloidal flows have been observed in the Alcator C-Mod tokamak. The flow velocities scale with the input rf power, and the toroidal rotation is generally more than a factor of 2 above the empirical intrinsic rotation scaling. The toroidal rotation appears in the inner plasma first and is largely independent of the antenna toroidal phase. The MC ICW is detected by PCI, and confirmed by TORIC simulations. Comparing the TORIC result to the experimental flow measurement suggests that the interaction of the MC ICW with ^{3}He may be the main flow drive mechanism. This ICRF MC flow drive may be applicable on ITER. The $E\times B$ shear generated by the rf driven flow may be marginally sufficient for confinement enhancement on Alcator C-Mod, and further experimental work will be performed to explore the new research opportunities using MC flow drive.

ACKNOWLEDGMENTS

The authors thank Dr. Paul Bonoli for his interest and encouragement in this work and also thank the Alcator C-Mod operation and ICRF groups. This research utilized the MIT Plasma Science and Fusion Center Theory Group parallel computational cluster.

This work was supported at MIT by U.S. DOE Cooperative under Agreement No. DE-FC02-99ER54512.

[1] P. Terry, Rev. Mod. Phys. **72**, 109 (2000).
[2] C. Craddock and P. Diamond, Phys. Rev. Lett. **67**, 1535 (1991).
[3] E. J. Strait, T. S. Taylor, A. D. Turnbull, J. R. Ferron, L. L. Lao, B. Rice, O. Sauter, S. J. Thompson, and D. Wróblewsk, Phys. Rev. Lett. **74**, 2483 (1995).
[4] J. E. Rice, A. Ince-Cushman, J. S. deGrassie, L.-G. Eriksson, Y. Sakamoto, A. Scarabosio, A. Bortolon, K. H. Burrell, B. P. Duval, C. Fenzi-Bonizec, M. J. Greenwald, R. J. Groebner, G. T. Hoang, Y. Koide, E. S. Marmar, A. Pochelon, and Y. Podpaly, Nucl. Fusion **47**, 1618 (2007).
[5] I. H. Hutchinson, J. E. Rice, R. S. Granetz, and J. A. Snipes, Phys. Rev. Lett. **84**, 3330 (2000).
[6] J. E. Rice, E. S. Marmar, P. T. Bonoli, R. S. Granetz, M. J. Greenwald, A. E. Hubbard, J. W. Hughes, I. H. Hutchinson, J. H. Irby, B. LaBombard, W. D. Lee, Y. Lin, D. Mossessian, J. A. Snipes, S. M. Wolfe, and S. J. Wukitch, Fusion Sci. Technol. **51**, 288 (2007).
[7] J. E. Rice, A. E. Hubbard, J. W. Hughes, M. J. Greenwald, B. LaBombard, J. H. Irby, Y. Lin, E. S. Marmar, D. Mossessian, S. M. Wolfe, and S. J. Wukitch, Nucl. Fusion **45**, 251 (2005).
[8] J. E. Rice, P. T. Bonoli, J. A. Goetz, M. J. Greenwald, I. H. Hutchinson, E. S. Marmar, M. Porkolab, S. M. Wolfe, S. J. Wukitch, and C. S. Chang, Nucl. Fusion **39**, 1175 (1999).
[9] M. Yoshida, M. Yoshida, Y. Koide, H. Takenaga, H. Urano, N. Oyama, K. Kamiya, Y. Sakamoto, and G. Matsunaga, Y. Kamada, and JT-60 Team, Nucl. Fusion **47**, 856 (2007).
[10] P. C. de Vries, M.-D. Hua, D. C. McDonald, C. Giroud, M. Janvier, M. F. Johnson, T. Tala, K.-D. Zastrow, and JET EFDA Contributors, Nucl. Fusion **48**, 065006 (2008).
[11] D. Nishijima, A. Kallenbach, S. Günter, M. Kaufmann, K. Lackner, C. F. Maggi, A. G. Peeters, G. V. Pereverzev, B. Zaniol, and ASDEX Upgrade Team, Plasma Phys. Controlled Fusion **47**, 89 (2005).
[12] P. A. Politzer, C. C. Petty, R. J. Jayakumar, T. C. Luce, M. R. Wade, J. C. DeBoo, J. R. Ferron, P. Gohil, C. T. Holcomb, A. W. Hyatt, J. Kinsey, R. J. La Haye, M. A. Makowski, and T. W. Petrie, Nucl. Fusion **48**, 075001 (2008).
[13] R. V. Budny, R. Andre, G. Bateman, F. Halpern, C. E. Kessel, A. Kritz, and D. McCune, Nucl. Fusion **48**, 075005 (2008).
[14] L.-G. Eriksson, E. Righi, and K.-D. Zastrow, Plasma Phys. Controlled Fusion **39**, 27 (1997).
[15] S. Assas, C. Fenzi-Bonizek, L.-G. Eriksson, and G. T. Hoang, 30th EPS Conference on Plasma Physics and Controlled Fusion, St. Petersburg, Russia, 7–11 July 2003 (unpublished), Vol. ECA 27A, p. 1.138.
[16] J. S. deGrassie, J. E. Rice, K. H. Burrell, and R. J. Groebner, Phys. Plasmas **14**, 056115 (2007).
[17] Y. Sakamoto, S. Ide, M. Yoshida, Y. Koide, T. Fujita, H. Takenaga, and Y. Kamada, Plasma Phys. Controlled Fusion **48**, A63 (2006).
[18] L. Porte, S. Coda, S. Alberti, G. Arnoux, P. Blanchard, A. Bortolon, A. Fasoli, T. P. Goodman, Y. Klimanov, Y. Martin, M. Maslov, A. Scarabosio, and H. Weisen, Nucl. Fusion **47**, 952 (2007).
[19] A. Ince-Cushman, J. E. Rice, M. Reinke, M. Greenwald, G. Wallace, R. Parker, C. Fiore, J. W. Hughes, P. Bonoli, S. Shiraiwa, A. Hubbard, S. Wolfe, I. H. Hutchinson, E. Marmar, M. Bitter, J. Wilson, and K. Hill, Phys. Rev. Lett. **102**, 035002 (2009).
[20] S. J. Wukitch, C. Litwin, M. Harper, R. Parker, and N. Hershkowitz, Phys. Rev. Lett. **77**, 294 (1996).
[21] B. P. LeBlanc, R. E. Bell, S. Bernabei, J. C. Hosea, R. Majeski, M. Ono, C. K. Phillips, J. H. Rogers, G. Schilling, C. H. Skinner, and J. R. Wilson, Phys. Rev. Lett. **82**, 331 (1999).
[22] J. R. Wilson, R. E. Bell, S. Bernabei, K. Hill, J. C. Hosea, B. LeBlanc, R. Majeski, R. Nazikian, M. Ono, C. K. Phillips, G. Schilling, S. von Goeler, C. E. Bush, and G. R. Hanson, Phys. Plasmas **5**, 1721 (1998).
[23] L.-G. Eriksson, T. Johnson, T. Hellsten, C. Giroud, V. G. Kiptily, K. Kirov, J. Brzozowski, M. DeBaar, J. DeGrassie, M. Mantsinen, A. Meigs, J.-M. Noterdaeme, A. Staebler, D. Testa, A. Tuccillo, and K.-D. Zastrow, Phys. Rev. Lett. **92**, 235001 (2004).
[24] C. K. Phillips, M. G. Bell, R. E. Bell, S. Bernabei, M. Bettenhausen, C. E. Bush, D. Clark, D. S. Darrow, E. D. Fredrickson, G. R. Hanson, J. C. Hosea, B. P. LeBlanc, R. P. Majeski, S. S. Medley, R. Nazikian, M. Ono, H. K. Park, M. P. Petrov, J. H. Rogers, G. Schilling, C. H. Skinner, D. N. Smithe, E. J. Synakowski, G. Taylor, and J. R. Wilson, Nucl. Fusion **40**, 461 (2000).
[25] Y. Lin, J. E. Rice, S. J. Wukitch, M. J. Greenwald, A. E. Hubbard, A. Ince-Cushman, L. Lin, M. Porkolab, M. L. Reinke, and N. Tsujii, Phys. Rev. Lett. **101**, 235002 (2008).
[26] T. H. Stix, *Waves in Plasmas* (American Institute of Physics, New York, 1992).
[27] M. Porkolab, AIP Conf. Proc. **314**, 99 (1994).
[28] E. Nelson-Melby, M. Porkolab, P. T. Bonoli, Y. Lin, A. Mazurenko, and S. J. Wukitch, Phys. Rev. Lett. **90**, 155004 (2003).
[29] F. W. Perkins, Nucl. Fusion **17**, 1197 (1977).
[30] Y. Lin, S. J. Wukitch, A. Parisot, J. C. Wright, N. Basse, P. Bonoli, E. Edlund, L. Lin, M. Porkolab, G. Schilling, and P. Phillips, Plasma Phys. Controlled Fusion **47**, 1207 (2005).

[31] Y. Lin, S. J. Wukitch, P. T. Bonoli, E. Marmar, D. Mossessian, E. Nelson-Melby, P. Phillips, M. Porkolab, G. Schilling, S. Wolfe, and J. Wright, Plasma Phys. Controlled Fusion **45**, 1013 (2003).
[32] J. C. Wright, P. T. Bonoli, M. Brambilla, F. Meo, E. D'Azevedo, D. B. Batchelor, E. F. Jaeger, and L. A. Berry, Phys. Plasmas **11**, 2473 (2004).
[33] M. Brambilla, Plasma Phys. Controlled Fusion **41**, 1 (1999).
[34] L. Lao, H. S. John, R. Stambaugh, A. G. Kellman, and W. Pfeiffer, Nucl. Fusion **25**, 1611 (1985).
[35] A. Ince-Cushman, J. E. Rice, M. Bitter, M. L. Reinke, K. W. Hill, M. F. Gu, E. Eikenberry, Ch. Broennimann, S. Scott, Y. Podpaly, S. G. Lee, and E. S. Marmar, Rev. Sci. Instrum. **79**, 10E302 (2008).
[36] J. Candy and R. E. Waltz, J. Comput. Phys. **186**, 545 (2003).
[37] W. D. Lee, J. E. Rice, E. S. Marmar, M. J. Greenwald, I. H. Hutchinson, and J. A. Snipes, Phys. Rev. Lett. **91**, 205003 (2003).
[38] L. Lin, E. M. Edlund, M. Porkolab, Y. Lin, and S. J. Wukitch, Rev. Sci. Instrum. **77**, 10E918 (2006).
[39] J. R. Myra and D. A. D'Ippolito, Phys. Plasmas **9**, 3867 (2002).
[40] L. A. Berry, E. F. Jaeger, and D. B. Batchlor, Phys. Rev. Lett. **82**, 1871 (1999).
[41] J. R. Myra, L. A. Berry, D. A. D'Ippolito, and E. F. Jaeger, Phys. Plasmas **11**, 1786 (2004).
[42] E. F. Jaeger, L. A. Berry, J. R. Myra, D. B. Batchelor, E. D'Azevedo, P. T. Bonoli, C. K. Phillips, D. N. Smithe, D. A. D'Ippolito, M. D. Carter, R. J. Dumont, J. C. Wright, and R. W. Harvey, Phys. Rev. Lett. **90**, 195001 (2003).
[43] Y. Lin, S. Wukitch, P. Bonoli, E. Nelson-Melby, M. Porkolab, J. C. Wright, N. Basse, A. E. Hubbard, J. Irby, L. Lin, E. S. Marmar, A. Mazurenko, D. Mossessian, A. Parisot, J. Rice, S. Wolfe, C. K. Phillips, G. Schilling, J. R. Wilson, P. Phillips, and A. Lynn, Phys. Plasmas **11**, 2466 (2004).
[44] E. F. Jaeger, L. A. Berry, E. F. D'Azevedo, R. F. Barrett, S. D. Ahern, D. W. Swain, D. B. Batchelor, R. W. Harvey, J. R. Myra, D. A. D'Ippolito, C. K. Phillips, E. Valeo, D. N. Smithe, P. T. Bonoli, J. C. Wright, and M. Choi, Phys. Plasmas **15**, 072513 (2008).
[45] T. S. Hahm and K. H. Burrell, Phys. Plasmas **2**, 1648 (1995).